Supplemental Material: Two-particle Interference with Double Twin-atom Beams

F. Borselli,[1] M. Maiwöger,[1] T. Zhang,[1] P. Haslinger,[1] V. Mukherjee,[2] A. Negretti,[3]
S. Montangero,[4,5] T. Calarco,[6] I. Mazets,[1,7] M. Bonneau,[1] and J. Schmiedmayer[1]

[1] *Vienna Center for Quantum Science and Technology, Atominstitut, TU Wien, 1020 Vienna, Austria*
[2] *Indian Institute of Science Education and Research, 760010 Berhampur, India*
[3] *The Hamburg Centre for Ultrafast Imaging, Universität Hamburg, D-22761 Hamburg, Germany*
[4] *Dipartimento di Fisica e Astronomia "G. Galilei", Università di Padova, I-35131 Padova, Italy*
[5] *INFN Sezione di Padova, I-35131 Padua, Italy.*
[6] *Forschungszentrum Jülich, Wilhelm-Johnen-Straße, D-52425 Jülich,*
and University of Cologne, Institute for Theoretical Physics, D-50937 Cologne, Germany
[7] *Research Platform MMM "Mathematics–Magnetism–Materials",*
c/o Fakultät für Mathematik, Universität Wien, 1090 Vienna, Austria

(Dated: December 9, 2020)

I. STATE INVERSION USING OPTIMAL CONTROL TECHNIQUES

The system consists of a quasi-one-dimensional condensate, i.e. a weakly interacting bosonic ensemble that is loosely confined longitudinally, but tightly confined transversally, as in previously realised optimal control experiments with atom chips [S1, S2]. In the transverse direction that hereafter we denote as the y-axis the potential is initially a single (anharmonic) well, as in Refs. [S1, S2], but then it is controlled dynamically by means of an external radio-frequency field in order to transform it to a double-well potential [S3]. As in previous related experiments [S1, S2], the system dynamics along the y-axis can be described through an effective one-dimensional Gross-Pitaevskii equation, whose nonlinear Hamiltonian is given by

$$\hat{H}_{\rm gp}[\psi,t] = -\frac{\hbar^2}{2m}\frac{\partial^2}{\partial y^2} + V(y,t) + gN|\psi(y,t)|^2. \tag{S.1}$$

Here, m is the mass of the boson, specifically of the alkali atom ^{87}Rb, $V(y,t)$ is the time-dependent potential that we manipulate optimally, g is the effective one-dimensional boson-boson coupling constant (see Ref. [S2] for further details), N is the number of bosons, and $\psi(y,t)$ is the condensate wavefunction formalised to unity. We note that because of the large separation of time scales between the transverse and longitudinal degrees of freedom, the quantum dynamics of the latter can be effectively assumed to be frozen during the excitation process in the transverse direction, which we are interested in.

The external potential $V(y,t)$ produced by the atom chip is approximated by

$$\begin{aligned} V(y,t) &= a_0(t) + a_2(t)y^2 + a_4(t)y^4 + a_6(t)y^6, \\ a_n(t) &= \sum_{j=1}^{6} \alpha_j^{(n)} [R_f(t)]^j \text{ for } n = 0,2,4,6, \end{aligned} \tag{S.2}$$

where the time-independent parameters $\alpha_j^{(n)}$, which are provided in Tab. S1, have units of kHz/m^n. The numerical values of the parameters $\alpha_j^{(n)}$ have been obtained by numerically fitting the simulated and experimentally calibrated potential generated by the atom chip with a polynomial of sixth order. This strategy has been adopted to simplify the numerical effort of the optimisation. The dimensionless time-dependent function $R_f(t)$ is proportional to the strength of the radio-frequency field applied to the atom chip and it is the control parameter we have to optimise.

In the present experiment, the quasi-condensate is initially prepared in the ground state, $\varphi_0(y)$, of the initial single well potential $V(y,0)$. Our goal is to bring the quasi-condensate in the second excited state, $\varphi_2(y)$, of the external potential $V(y,t_f)$ in double-well configuration in a time t_f shorter than the decoherence time of the system. Here, the nonlinear eigenstates $\varphi_{0,2}(y)$ of the Hamiltonian (S.1) are determined numerically by the imaginary-time technique with $N = 700$. To this end, we employ optimal control techniques to generate the optimal radio-frequency field $R_f(t)$ that minimises the cost function defined at the final time t_f as

$$\mathcal{J} = 1 - \left| \int_{\mathbb{R}} {\rm d}y\, \varphi_2^*(y)\psi(y,t_f) \right|^2. \tag{S.3}$$

j	$\alpha_j^{(0)}$	$\alpha_j^{(2)}$	$\alpha_j^{(4)}$	$\alpha_j^{(6)}$
0	54.451	74.025	-3.4221	0.2406
1	-8.6264	-19.429	24.648	-6.0581
2	3570.3	- 3309.1	1231.6	-153.85
3	-12650	18497	-8450.8	1221.2
4	25646	-46369	23425	-3661.4
5	-27546	56311	-30416	5049.5
6	12106	-26894	15268	-2663.3

Table S1. The parameters $\alpha_j^{(n)}$ in units of kHz/μm^n for $n = 0, 2, 4, 6$.

Specifically, we employ the CRAB optimisation method [S4]. Here, the radio-frequency field $R_f(t)$ is expanded into a (not necessarily orthogonal) truncated basis

$$R_f(t) = 0.3 + \frac{1}{\lambda(t) N_f} \left| \sum_{j=1}^{N_f} \left(c_j \cos \frac{2\pi f_j t}{t_f} + d_j \sin \frac{2\pi f_j t}{t_f} \right) \right| + 0.21\, e^{-8(t_f - t)}, \tag{S.4}$$

for $0 \leq t \leq t_f$. Here $N_f = 10$ denotes the total number of frequencies considered in Eq. (S.4); the multiple frequencies allow us to engineer non-trivial pulses with multiple maxima and minima, as shown in Fig. S1. The dimensionless function

$$\lambda(t) = 0.5 + 10^4 \left[e^{-8t} + e^{-8(t_f - t)} \right] \tag{S.5}$$

is large and positive at $t = 0$, t_f, thereby fixing the initial and final values of the RF-field. On the other hand,

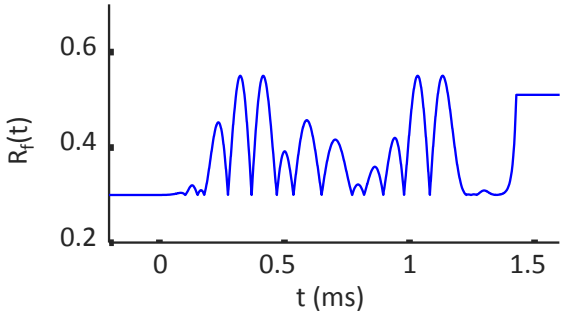

Figure S1. The ramp $R_f(t)$ of the amplitude of the radio-frequency field against time.

$\lambda(t)$ assumes the value 0.5 at intermediate times, so as to allow for variations of the RF-field within the interval $(0, t_f)$. Furthermore, owing to experimental constraints, we impose the condition $0.3 \leq R_f(t) \leq 0.55\ \forall\ t$. We note that the field (S.4) is already given in dimensionless units, where times are rescaled with respect to $1/\omega_0$. The optimisation is carried out by varying the parameters c_j, d_j and f_j. Thus, the optimisation has been performed in such a way that the double-well potential $V(y, t_f)$ is obtained by setting $R_f(t_f) = 0.51$ at final time $t_f/\omega_0 = 1.4$ ms, while $R_f(0) = 0.3$ results in the initial single-well potential. The exponential function appearing in Eq. S.4 and its width 1/8 have been chosen such that it increases smoothly and monotonically to the numerical value 0.21 as $t \to t_f^-$, such that the control parameter reaches the target value $R_f(t_f) = 0.51$ and we avoid excitation of the condensate along the vertical z-axis. In Fig. S1 the optimised curve of the parameter $R_f(t)$ is plotted against time. The values of $R_f(t)$ for $t < 0$ and $t > t_f = 1.4$ ms in Fig. S1 signify that $R_f(t)$ is time-dependent only for the intermediate optimization times $(0, t_f)$, while it assumes constant values outside this time-interval.

A. Transfer efficiency

We estimate the percentage of atoms transferred to the source state from the evolution of the wavefunction of the BEC after the excitation pulse. If more than one eigenstate of the potential are populated, we should observe a beating pattern in the momentum distribution varying with the holding time in the trap. If the excited wavefunction corresponds to the source state, which is an eigenstate of the double-well potential, the outcome would be a constant profile. The experimental profile was fitted with a linear combination $\Psi_{guess}(y)$ of different single-particle eigenstates $\psi_i(y)$ up to the sixth order ($i = 6$):

$$\Psi_{guess}(y) = p_2\psi_2(y) + \sum_i e^{i\phi_i}\sqrt{p_i}\psi_i(y) \tag{S.6}$$

where ϕ_i ($i = 0, 1, 4, 6$) are the relative phases and p_i ($i = 0, 1, 2, 4, 6$) are the normalized contributions from the five different states considered. The odd components from the third and fifth order were excluded from the fit function based on symmetry arguments to reduce the number of free parameters. This is consistent with the transverse symmetry of the experimental data. The main contribution to the experimental profile comes from the second excited state of the double-well potential ($\sim 97\%$), corresponding to the source state. This demonstrates the state inversion using the optimal control engineered sequence.

II. CREATION OF THE DTB STATE

A wave function $\Psi(\mathbf{r}_1, \mathbf{r}_2) \equiv \Psi(x_1, y_1, z_1; x_2, y_2, z_2)$ of two spin-polarized bosonic atoms is symmetric with respect to the permutation of the coordinates (x_1, y_1, z_1) and (x_2, y_2, z_2) of these atoms. If we factorize it into the longitudinal ($\parallel$) and transverse ($\perp$) parts, $\Psi(x_1, y_1, z_1; x_2, y_2, z_2) = \Psi_\parallel(x_1; x_2)\Psi_\perp(y_1, z_1; y_2, z_2)$ we readily see that each of them must be symmetric with respect to the permutation of its coordinates, $\Psi_\parallel(x_1; x_2) = \Psi_\parallel(x_2; x_1)$ and $\Psi_\perp(y_1, z_1; y_2, z_2) = \Psi_\perp(y_2, z_2; y_1, z_1)$, in order to be non-zero at $\mathbf{r}_1 = \mathbf{r}_2$, thus allowing for s-wave scattering on the two-atom contact interaction (pseudo)potential $\propto \delta(x_1 - x_2)\delta(y_1 - y_2)\delta(z_1 - z_2)$, where δ is the Dirac delta-function. We can write the initial state of the two particles in the spatial basis as

$$\Psi_{in}(x_1, y_1, z_1; x_2, y_2, z_2) = \langle y_1, z_1|2\rangle\langle y_2, z_2|2\rangle\langle x_1|k_x = 0\rangle\langle x_2|k_x = 0\rangle, \tag{S.7}$$

where $|n_y\rangle = |2\rangle$ represents the transverse second-excited state and we assumed that longitudinally only the $|k_x = 0\rangle$ mode is initially populated (the source state is at rest longitudinally).

The emission process conserves the symmetry of the initial two-particle wavefunction. However, the $\delta(x_1 - x_2)$ term precludes transitions into antisymmetric longitudinal states. Therefore, only the longitudinal state $(\langle x_1| - k_0\rangle\langle x_2|k_0\rangle + \langle x_2| - k_0\rangle\langle x_1|k_0\rangle)/\sqrt{2}$ is possible. For the transverse component of the final wavefunction, let us consider the $\{|L\rangle, |R\rangle\}$ basis. Due to bosonic symmetry, the transverse state is also symmetric with respect to the exchange of transverse coordinates. However, transitions to $|LR\rangle$ or $|RL\rangle$ are not possible, since

$$\begin{aligned}\int dy_1 \int dy_2 \int dz_1 \int dz_2\, \langle 2|y_1, z_1\rangle\langle 2|y_2, z_2\rangle\delta(y_1 - y_2)\delta(z_1 - z_2)\frac{\langle y_1, z_1|L\rangle\langle y_2, z_2|R\rangle + \langle y_1, z_1|R\rangle\langle y_2, z_2|L\rangle}{\sqrt{2}} \\ = \sqrt{2}\int dy \int dz\, (\langle 2|y, z\rangle)^2\langle y, z|L\rangle\langle y, z|R\rangle = 0\end{aligned} \tag{S.8}$$

due to negligible overlap between the states $|L\rangle$ and $|R\rangle$.

The remaining symmetric transverse states are $\left|\Psi_\perp^-\right\rangle = (|LL\rangle - |RR\rangle)/\sqrt{2}$ and $\left|\Psi_\perp^+\right\rangle = (|LL\rangle + |RR\rangle)/\sqrt{2}$. Since for a perfectly symmetric trap

$$\int dy \int dz\, (\langle 2|y, z\rangle)^2(\langle y, z|L\rangle)^2 = \int dy \int dz\, (\langle 2|y, z\rangle)^2(\langle y, z|R\rangle)^2, \tag{S.9}$$

the matrix element for a transition from $|2\rangle|2\rangle$ to $\left|\Psi_\perp^-\right\rangle$ vanishes due to destructive interference. The only non-zero matrix element couples $|2\rangle|2\rangle$ to $\left|\Psi_\perp^+\right\rangle$. Taking into account also the longitudinal component $(e^{-ik(x_1-x_2)} + e^{-ik(x_2-x_1)})/\sqrt{2}$, we recover the DTB state $|\Psi_{DTB}\rangle = (|L\rangle_-|L\rangle_+ + |R\rangle_-|R\rangle_+)/\sqrt{2}$.

	Separation		Interference
t_{hold}(ms)	0.025	0.425	0.025
Total images	684	825	1498
$\tilde{\xi}^2_{k_0/-k_0}$	0.18	0.22	0.30
$\xi^2_{k_0/-k_0}$	0.10(1)	0.14(1)	0.10(1)

Table S2. **Twin character** Main parameters of the two sets of data considered in this paper: the uncorrected atom number-squeezing factor $\tilde{\xi}^2_{k_0/-k_0}$ and the noise-corrected one $\xi^2_{k_0/-k_0}$. The latter is an indicator of the twin character of the DTB emission, i.e. the process of creation of pairs of atoms carrying opposite momenta.

A. Extension to a fermionic system

In our present experiment the source state from where the atom pairs are emitted relies on a Bose-Einstein condensate which has a defined longitudinal momentum $k_x = 0$. Moreover, the emitted double twin-atom beams are created by an s-wave scattering process. The same procedure does not apply to a fermionic gas. The atoms in a fermionic source state would have many longitudinal momenta up to the Fermi momentum k_F and the total momentum of the emitted atom pairs would be not well defined. Moreover, spin-polarized fermions do not experience s-wave scattering, hence the collisional process at the basis of the emission of twin-beams would be completely different. So a source of fermionic twin atoms would have to look completely different. One can imagine breaking up a bosonic diatomic Feschbach molecule into its fermionic components as for example proposed as source for entangled atom pairs in [S5], but imprinting a significant momentum on them would require additional processes like transferring the molecule before the break-up into a higher excited quasi bound state. We could then envision such a system that produces twin fermionic atoms in a single waveguide. The spin degree of freedom would replace the double waveguide transverse degree of freedom of our setup and the emitted state would be a maximally entangled spin state $|\Phi^-\rangle = (|\downarrow\rangle_- |\uparrow\rangle_+ - |\uparrow\rangle_- |\downarrow\rangle_+)/\sqrt{2}$.

III. TWIN CHARACTER AND TOTAL TRANSVERSE SQUEEZING

As already done in [S6], we check the twin character of the DTB emission by looking at the fluctuations of the difference photon number S_- between the atoms with momentum $\pm k_0$ over the different experimental realizations. For the separation data, we simply integrate over the two transverse modes $S_- = (S_{L_-} + S_{R_-}) - (S_{L_+} + S_{R_+})$, where S_{L_-} is the signal contained in the black box L_- in Fig. 2a corresponding to the single-particle mode $|L_-\rangle$ (and similarly for the others). If there is no correlation among the signals in the two zones that are being analysed, the signal difference follows a binomial distribution. We can then evaluate the number squeezing factor $\xi^2_{k_0/-k_0}$ between the two longitudinal momentum classes and classify $\xi^2_{k_0/-k_0} < 1$ as a number-squeezed emission. The main information about the data are listed in Tab. S2. In particular, the results on the noise-corrected $\xi^2_{k_0/-k_0}$ between the two momentum states $\pm k_0$ confirm the results in [S6], thus demonstrating the presence of a strongly non-Poissonian amount of correlations between the DTBs of opposite momenta. The error on ξ^2 is estimated using a bootstrapping method comparing 50 statistical copies of the full experiment.

We can also consider the total transverse number squeezing, i.e. the signal difference between the number of pairs emitted in the L- and in the R-waveguide, after integrating on the two longitudinal momenta (see light-blue dashed boxes in Fig. 2b). Since the atoms are detected pairwise independently into the L- and R-waveguide, we expect the distribution of the pairs difference M_- to be binomial (uncorrelated). Hence, if M_+ is the total number of pairs, the corresponding variance is $\Delta M_-^2 = M_+$. Let us now consider the distribution of the signal difference N_- between the atoms in the L-waveguide and R-waveguide and its variance ΔN_-^2. Since $var(aX) = a^2 var(X)$ for any variable X where a is a constant, we get $\Delta N_-^2 = \Delta^2(2M_-) = 4\Delta N_-^2 = 4M_+ = 2N_+$. From this follows that $\xi^2_{L/R} \equiv \Delta N_-^2/\Delta_b N_-^2 = (2N_+)/N_+ = 2$.

IV. IMAGING SYSTEM

Our fluorescence based imaging system consists of a nearly resonant sheet of light made of two counter-propagating laser beams. The light-sheet excites the atoms and make them undergo several absorption-spontaneous

emission cycles. Part of these photons are collected on a camera placed below the atom chip and converted into electrons. In principle, single atom recognition is possible and was already demonstrated in this system [S7]. If the two counter-propagating laser beams are not exactly overlapped, or if their power is unbalanced, a light-pressure effect can show up in the fluorescence picture. For the data considered in this paper this effect is only residual (Fig. 2a). We take pictures after a time-of-flight $t_{TOF} = 44\,\mathrm{ms}$.

A. Far-field regime for the transverse direction

The final position x_F of a trapped particle along a certain spatial direction x after its release from the trap at time $t = 0$ and a time-of-flight $t_{TOF} \equiv t_F$ reads $x_F = x_0 + \dot{x}_0 \cdot t_F = x_0 + p_0/m \cdot t_F$, where x_0 ($\dot{x}_0 = p_0/m$) represents the initial position (velocity) of the particle in the trap at the moment of the release and p_0 its initial momentum. Assuming a harmonic trapping ($\dot{x} = i\omega_x x$) with angular frequency ω_x along the x-axis, we derive the expression $x_F = x_0 + i\omega_x x_0 \cdot t_F = x_0 + p_0/m \cdot t_F$. The condition of the final position expressing the initial momentum of the particle in the trap at the moment of the release is then $p_0/m \cdot t_F \gg x_0$, which translates into the requirement $i\omega_x x_0 \cdot t_F \gg x_0 \rightarrow t_F \gg 1/\omega_{x,y,z}$, independently of the spatial direction we are referring to. In our experimental setup we have $\omega_x \simeq 2\pi \cdot 10$ Hz and $\omega_{y,z} = 2\pi \cdot 2$ kHz, which corresponds to $1/\omega_x \simeq 16$ ms and $1/\omega_{y,z} \simeq 0.1$ ms. Since in our setup $t_F = 44$ ms, the condition $t_F \gg 1/\omega_{x,y,z}$ is well satisfied along the transverse y,z-axis and only partly satisfied along the x-axis. This shows that the transverse expansion of the atomic cloud after its release from the chip trap is fast compared to t_{TOF}, hence the fluorescence image of the final cloud shows the in-situ momentum distribution along the y-axis.

B. Atom detection and detection noise

Experimentally we cannot access the atom number directly, but rather we measure the number of photons hitting the camera. Having considered two boxes 1 and 2 on a typical fluorescence image (consider for example any two black boxes in Fig. 2a), we define the sum and difference photon signal relative to the two boxes $S_\pm = S_1 - S_2$, where S_1 (S_2) is the measured fluorescence signal from box 1 (2). If we assume that to each imaged atom correspond exactly p photons, then we can write

$$S_\pm = pN_\pm, \tag{S.10}$$

where $N_\pm$ is the sum or difference atom number relative to the same two boxes. Having assumed p constant, we can derive an expression for the variance of the signal difference $\Delta S_-^2 \equiv \mathrm{var}(pN_-) = p^2 \Delta N_-^2$. Using Eq. S.10 and the expression $\Delta_b N_-^2 = N_+$ we get

$$\tilde{\xi}^2 \equiv \frac{\Delta N_-^2}{\Delta_b N_-^2} \equiv \frac{p^2}{p^2} \cdot \frac{\Delta N_-^2}{N_+} = \frac{\Delta S_-^2}{pS_+}. \tag{S.11}$$

In order to evaluate the average number of photons p scattered by each atom, we compare fluorescence images to absorption images for increasingly larger atomic clouds [S8]. From this comparison, we derived $p = 29.4$ for the separation data and $p = 20.7$ for the interference data, meaning each atom is generating, on average, clusters of around 20-30 photons when crossing the light-sheet. We come now to the discussion on detection noise [S9]. The final number of counts created by each photon hitting the camera is a random variable, whose statistics is governed by photonic shot noise. On top of the usual shot noise level, there is an additional noise generated by the amplification stage at the electron-multiplication register of the camera. To account for it, the variance due to shot noise gets doubled [S10]: $\Delta_{sn} S_-^2 = 2S_+$. A second contribution comes from the background signal $\hat{b}$ contained in a certain area of the camera chip, which is important when regions with low signal are considered. Since the background signal is indistinguishable from the actual signal coming from the atomic fluorescence, the same considerations made above apply and $\Delta_{sn} b_-^2 = 2b_+$. We define the total noise contribution to the variance $\Delta_n S_-^2 = \Delta_{sn} S_-^2 + \Delta_{sn} b_-^2$ and modify the expression for the uncorrected number squeezing to take into account the total noise as

$$\xi^2 = \frac{\Delta S_-^2 - \Delta_n S_-^2}{\Delta_b S_-^2}. \tag{S.12}$$

We can then define the minimum value of atom number squeezing ξ_n^2 between the momentum states detectable in our system as

$$\xi_n^2 = \frac{\Delta_n S_-^2}{\Delta_b S_-^2} = \frac{2S_+ + 2b_+}{pS_+} \simeq 2/p, \quad \text{for } b_+ \ll S_+. \tag{S.13}$$

Typical values are $\xi_n^2 \simeq 0.08$ (separation data) and $\xi_n^2 \simeq 0.2$ (interference data). The difference can be explained by the different signal-to-noise ratio S_+/b_+ for the two datasets.

V. ONE-DIMENSIONAL FIT OF THE SECOND-ORDER CORRELATION FUNCTION

The one-dimensional fringe pattern of $g^{(2)}_{exp}(k_-^y, k_+^y)$ is fitted using the fit-function

$$f(k_y) = \left[d + C\cos\left(2\pi\frac{k_y - K}{e_{exp}}\right)\right]\exp\left[\frac{-(k_y-K)^2}{(c_{sigma}/e_{exp})^2}\right], \tag{S.14}$$

where K is the coordinate of the centre of the fringe pattern, c_{sigma} is a dimensional parameter, e_{exp} represents the diagonal fringe spacing, $C = 0.032 \pm 0.004$ is the contrast of the fringe pattern and d an offset.

[S1] S. van Frank, A. Negretti, T. Berrada, R. Bücker, S. Montangero, J.-F. Schaff, T. Schumm, T. Calarco, and J. Schmiedmayer, Nature communications **5**, 1 (2014).

[S2] S. van Frank, M. Bonneau, J. Schmiedmayer, S. Hild, C. Gross, M. Cheneau, I. Bloch, T. Pichler, A. Negretti, T. Calarco, *et al.*, Scientific reports **6**, 34187 (2016).

[S3] I. Lesanovsky, T. Schumm, S. Hofferberth, L. M. Andersson, P. Krüger, and J. Schmiedmayer, Physical Review A **73**, 033619 (2006).

[S4] T. Caneva, T. Calarco, and S. Montangero, Phys. Rev. A **84**, 022326 (2011).

[S5] B. Zhao, Z.-B. Chen, J.-W. Pan, J. Schmiedmayer, A. Recati, G. E. Astrakharchik, and T. Calarco, Physical Review A **75**, 042312 (2007).

[S6] R. Bücker, J. Grond, S. Manz, T. Berrada, T. Betz, C. Koller, U. Hohenester, T. Schumm, A. Perrin, and J. Schmiedmayer, Nature Physics **7**, 608 (2011).

[S7] R. Bücker, A. Perrin, S. Manz, T. Betz, C. Koller, T. Plisson, J. Rottmann, T. Schumm, and J. Schmiedmayer, New Journal of Physics **11**, 103039 (2009).

[S8] M. Pigneur, *Non-equilibrium Dynamics of Tunnel-Coupled Superfluids: Relaxation to a Phase-Locked Equilibrium State in a One-Dimensional Bosonic Josephson Junction* (Springer Nature, 2020).

[S9] R. Bücker, *Twin-atom beam generation in a one-dimensional Bose gas*, Ph.D. thesis, Techische Universität Wien (2013).

[S10] A. Basden, C. Haniff, and C. Mackay, Monthly notices of the royal astronomical society **345**, 985 (2003).